# Advanced Thermal Barrier Coating Development and Testing

RELATION OF THERMAL CONDUCTIVITY WITH PROCESS INDUCED ANISOTROPIC VOID SYSTEMS IN EB-PVD PYSZ THERMAL BARRIER COATINGS

A. Flores Renteria, B. Saruhan
Institute of Materials Research,
German Aerospace Center
Linder Hoehe, Porz-Wahnheide
Cologne, NRW 51147, Germany

J. Ilavsky
X-Ray Operations and Research (XOR), Experimental Facilities Division,
Advanced photon Source (APS)
Argonne National Laboratory
9700 S. Cass Avenue, bldg 438E
Argonne, IL 60439, USA

ABSTRACT

Thermal barrier coatings (TBCs) deposited by Electron-beam physical deposition (EB-PVD) protect the turbine blades situated at the high pressure sector of the aircraft and stationary turbines. It is an important task to uphold low thermal conductivity in TBCs during long-term service at elevated temperatures. One of the most promising methods to fulfil this task is to optimize the properties of PYSZ-based TBC by tailoring its microstructure. Thermal conductivity of the EB-PVD produced PYSZ TBCs is influenced mainly by the size, shape, orientation and volume of the various types of porosity present in the coatings. These pores can be classified as open (inter-columnar and between feather arms gaps) and closed (intra-columnar pores). Since such pores are located within the three-dimensionally deposited columns and enclose large differences in their sizes, shapes, distribution and anisotropy, the accessibility for their characterization is very complex and requires the use of sophisticated methods. In this work, three different EB-PVD TBC microstructures were manufactured by varying the process parameters, yielding various characteristics of their pores. The corresponding thermal conductivities in as-coated state and after ageing at 1100C/1h and 100h were measured via Laser Flash Analysis Method (LFA). The pore characteristics and their individual effect on the thermal conductivity are analysed by USAXS which is supported by subsequent modelling and LFA methods, respectively. Evident differences in the thermal conductivity values of each microstructure were found in as-coated and aged conditions. In summary, broader columns introduce higher values in thermal conductivity. In general, thermal conductivity increases after ageing for all three investigated microstructures, although those with initial smaller pore surface area show smaller changes.

INTRODUCTION

Attractive thermo mechanical properties of electron beam - physical vapour phase deposited (EB-PVD) thermal barrier coatings (TBCs) are attributed to their unique microstructure. The primary columns present in these microstructures are separated by inter-columnar gaps oriented perpendicular to the substrate's plane, leading to excellent thermo-shock resistance of these coatings under thermal cyclic conditions. It is noteworthy that the inter-columnar gaps are oriented parallel to the heat flux, and thus, unfavourable for the capability of the TBCs as thermal insulators. The heat flux is principally transported through the solid column material being equilibrated by intra-columnar pores and voids between feather-arms.

During the EB-PVD coating process, primary columns start to grow on the substrate surface following a nucleation stage. The columnar growth occurs in a preferred direction, typically perpendicular to the plane of the substrate. Inter-columnar gaps and feather-arm features are created due to the shadowing effect of the neighbouring column tips which impede the vapour flux to reach the bottom of the valley between the columns[1]. Moreover, the formation and growth of the voids between feather-arms are influenced by the next factors:

(a) The sunshine-sunset shadowing effect of the neighbouring columns tips, resulting in different morphological sequences at the directions parallel and perpendicular to the plane of vapour incidence (PVI);

(b) The substrate temperature, that regulates the diffusion of atoms at the growing surface and

(c) The rotation speed, influencing the solid material growth and yielding the "banana" shape pores due to shadowing after each completed rotation movement.

Since the feather-arm gaps are located at the periphery of the columns, the column-tip shadowing effect will be enhanced during the growing process with the support of the other two mentioned factors (i.e. those given by b and c). Therefore, this phenomenon is significant at the ultimate edge of the columns, forming their conical cross section. For this reason, the feather-arm gaps can be designated as open intra-columnar pores created at the columns periphery due to lower vapour flux available for the complete solid material deposition. In addition, intra-columnar pores are created inside the columns at regions of highest vapour incidence angles (VIA), where the edge of the deposited vapour after each complete rotation overlaps with the initial growth generated by the next rotation's movement. They grow through the deposited material parallel to the feather-arms in an elongated "banana" shape following the altered direction of the vapour incidence angle (VIA) in a sunrise-sunset pattern.

Thermal exposure of the EB-PVD deposited TBCs results in morphological changes which consequently affect the properties such as thermal conductivity and Young's Modulus. These may be due to the occurrence of a series of thermal processes varying from formation of bridges between the columns, formation of sintering necks at contact points between the feather-arms, and eventually changes in pore geometry and sizes of the intra-columnar pores[2]. All these thermally activated processes generate surface area reduction and may follow in a similar way as the sintering processes[3].

Previous studies[4-6] indicate that the microstructural configuration of the EB-PVD PYSZ TBCs significantly contribute to the intrinsic thermal properties of the material. Thus, the quantitative information on the spatial and geometrical characteristics of the pores within these coatings is required to correlate those with their thermal properties. Sophisticated techniques such as USAXS and USANS have shown to be effective in thorough characterization of as-coated EB-PVD TBCs[7-9]. However, no study is known up-to-date which benefits from these

techniques to determine the morphological alterations on ageing and to precisely identify the role of each morphological feature and alteration on the in-service stability of the thermal conductivity in EB-PVD manufactured PYSZ TBCs.

In this study, three different microstructures of EB-PVD produced PYSZ TBCs were manufactured by altering coating process parameters. Their morphological characterization was carried out in as-coated and aged (1100°C/100h) conditions via Ultra Small-Angle X-rays Scattering Method (USAXS). The measurements were carried out in two orthogonal directions per specimens due to the anisotropy of the pores. The resulting raw data were fitted employing a computer based model[10] capable to determine the mentioned characterization of the pores; i.e., volume, size, aspect ratio, shape and orientation of the inter-columnar gaps, gaps between feather-arms, and intra-columnar pores. Correspondingly, thermal conductivity of specimens under the same conditions was measured via Laser Flash Analysis Method (LFA).

MATERIALS AND METHODS

Materials and Processing

Partially Yttria Stabilized Zirconia (PYSZ) coatings were manufactured via EB-PVD process by employing "von Ardenne" pilot plant equipment having a maximum EB-power of 150 kW. Evaporation was carried out from a single evaporation source having the ingot dimensions of 62.5 mm diameter and 150 mm length. The chemical composition of the ingot was standard 7-8 wt.%$Y_2O_3$ stabilized $ZrO_2$. Deposition of the vapor phase on flat substrates was carried out under conventional rotating mode by mounting the substrates on a holder with its horizontal axis perpendicular to the evaporation source as described in[11] (i.e. perpendicular to PVI). During the coating process, the substrates were rotated at different speeds and heated to different temperatures (Table I). Table I lists the designation of the samples and the applied process parameters to manufacture these three investigated EB-PVD-morphologies.

**Table I.** EB-PVD coating conditions and designation for the three manufactured microstructures

| Morphology | Chamber Pressure (mbar) | Substrate Temperature (°C) | Rotation Speed (rpm) |
|---|---|---|---|
| Feathery | $8 \times 10^{-3}$ | 850 | 30 |
| Intermediate | $8 \times 10^{-3}$ | 950 | 12 |
| Coarse | $8 \times 10^{-3}$ | 1000 | 3 |

For USAXS characterization, the EB-PVD PYSZ coatings of app. 400 μm thickness were deposited on Ni-basis substrates which were previously coated with a NiCoCrAlY bond coat. USAXS specimens were prepared by cutting and polishing the coatings into 200μm thickness slices. Two orthogonal slices (e.g. perpendicular and parallel to the PVI) per specimen were obtained through this process. For thermal conductivity characterization by Laser-Flash-Analysis (LFA), the coatings were deposited on 12.7 mm diameter discs of FeCrAl-alloys (without bond coat) in the same run. For LFA sample preparation, the FeCrAl-alloy substrates were chemically etched to obtain coatings in free-standing conditions. Finally, these free-standing coatings were additionally coated on both sides with a thin Pt-layer via sputter method to avoid laser penetration during the measurements. Subsequently, corresponding specimens were heat treated in air at 1100°C/100h using a heating rate of 5°C/min.

Methods of Characterization

Microstructural Characterization
        The coating microstructures were characterized visually by using a Field-Emission Scanning Electron Microscope (FE-SEM, LEITZ LEO 982).

Ultra-Small Angle X-ray Scattering (USAXS)
        The effective pinhole-collimated USAXS instrument which is equipped with a data processing system and available at the UNICAT 33-ID of the Advance Photon Source, ANL, was employed for our measurements[8]. Effective-pinhole USAXS enables the characterization of anisotropic microstructures with nearly the same resolution previously available for isotropic materials. This instrument utilizes the advantages of Bonse-Hart[12] double-crystal diffraction optics to extend its range of the scattering vector Q (Q = $(4\pi/\lambda)(\sin \theta)$, where $\lambda$ is the wavelength of the incident X-rays and $2\theta$ is the scattering angle) to noticeably lower values ($1,2 \times 10^{-4}$ Å$^{-1}$ < $|Q| < 0,1$ Å$^{-1}$) by decoupling the resolution of the instrument from the primary beam size. This effective-pinhole configuration allows the measurement of the scattering vector (Q) in one direction (1D), which is perpendicular to the substrate's plane within the plane of the coating. Therefore, to determine the 2D distribution of the scattering intensities, rotation of the specimens in small increments of an azimuthal angle ($\alpha$) is required.
        In order to obtain the complete characterization of spatial and geometrical anisotropic microstructures such as EB-PVD TBCs, two measuring methods are usually employed:
(1) The scattering intensity, I(Q) is measured as function of the azimuthal angle ($\alpha$) for a constant Q value (aniso-scans) to determine the principal max. and min. scattering intensities and their respective $\alpha$ values;
(2) The scattering intensity (I(Q)) is measured as a function of Q at the principal $\alpha$ values.
By combining the results obtained by these methods a quantitative map of the microstructural anisotropy as function of the pore sizes can be done[8].
        Since the analyzed coatings enclose anisotropic stereometric characteristics at the azimuthal and polar spatial domains, each specimen was measured at two orthogonal directions (perpendicular and parallel to the plane of vapor incidence). Several (i.e. five) aniso-scans at different fixed Q-values were done, which allowed the characterization of the complete size range of the pores within the coatings. Additionally, the scattering intensity at important anisotropic azimuthal orientations was measured.
        Scattering form-factor functions have been already derived for different shapes of scattering elements such as spheroids, rods, discs, networks, etc. and reported in previous studies [13-16]. Moreover, it is known that the scattering structure-factor function is dependent of local order, describing spatial correlations that may exist between scattering elements, e.g. monodispersed population of spherically shaped scatterers[17], arrays of parallel cylindrical shaped scatterers[18], or a fractal system[19]. Since real stereometric characteristics of every pore population enclose a certain deviation, the applied model considers Gaussian distribution for the calculation of the orientation and size values. It uses idealized particle shapes for which small-angle scattering can be reasonably well calculated (e.g. as ellipsoidal oblate and prolate, and spheres), and allows the optimization of the parameters by a last square fitting as given in[10]. The model allows the use of five independent pore populations composed of individual spheroid shapes with $R_0$, $R_0$ and $\beta R_0$ axes. In the employed coordinate system the x axis, and y and z axes lay perpendicular (in other words; parallel to the column axis), and parallel to the substrate's plane,

respectively. Furthermore, the orientation of the pores in the space is described by its $\beta R_0$ axis with respect to the coordinate system by two independent angles $\alpha$ (azimuthal angle) and $\omega$ (polar angle). An anisotropic orientation model was applied in a study[7] which assumes the solution of the differential scattering cross-section as function of the orientation for each scattering pore population. Due to uncertainties in the calibration of the USAXS-specimens thickness, the total volumes of the pores were measured by Archimedes Method. Thus, in this work, the USAXS-model predicts the volume fraction of each pore population.

Laser Flash Analysis Method (LFA)
        The thermal diffusivity of the Pt-coated free-standing specimens was measured employing a Netsch-LFA 427 instrument. The calculation of the thermal conductivity was calculated through the formula:

$$\lambda = \alpha \cdot \rho \cdot C_p \qquad (5)$$

Where, $\lambda$ is the thermal conductivity (W/m·K), in this case $\rho$ represents the bulk density (gr/cm$^3$) of the free-standing coatings measured by Archimedes Method and Cp is the specific heat (J/g·K) measured by Differential Scanning Calorimeter (DSC).

RESULTS AND DISCUSSION
        Microstructural observation of the coatings in the as-coated state displays the typical EB-PVD PYSZ morphology for all three intended microstructures. The main differences are being in the column diameter and in the feather-arm feature configuration. The microstructure "coarse" showed larger column diameters and the microstructure "feathery" more defined feather-arm features (Fig. 1). The resulting volume fractions of each pore population calculated with the USAXS-model were scaled to the corresponding total volume measured with Archimedes Method for each microstructure, which were 27.46% for the "feathery", 27.15% for the "intermediate", and 22.55% for the "coarse", respectively. As SEM micrographs also indicate, USAXS analysis deliver numerical data on the fact that basically all investigated microstructures show variations in their pore distribution and in their column density at the cross-sections, perpendicular and parallel to the plane of vapour incidence (PVI). At all three analysed coating, in the as-coated state, the inter-columnar gaps are slightly broader, and contain evidently higher volumes at the direction perpendicular to the plane of vapour incidence (PE-PVI) compared with that at the parallel direction (PA-PVI). This can also be observed in the micrographs shown in Fig. 1. As a matter of fact, some previous studies has delivered similar qualitative results solely relying on microstructural investigations[1].
        For simplicity purposes in this context, we compared the quantitative data obtained on the cross-sections of three investigated microstructures perpendicular to PVI (PE-PVI). Fig. 2 shows the measured and modeled polar distribution of the scattered intensities versus the azimuthal angle ($\alpha$) at different scattering vector (Q) values for as-coated state of the "coarse" microstructure (top row) and after ageing at 1100°C/100h (bottom row). The intensities drawn with symbols are fittings obtained by modeling. It has to be realized that the scattering intensities corresponding to the different mean opening dimensions (MOD) include scatterings with a specific range of similar sizes. The model uses Gaussian distribution averaging "size distribution" of 40-60%. Scattering intensities oriented at 90° and 270° azimuthal angles correspond to the inter-columnar gaps; while, the scattering intensities at 45-54° and 225-245°

azimuthal angles correspond to those from the feather-arms as well as intra-columnar pores which typically align behind the feather-arm features.

The results of the USAXS-modeling are given in Table II. The obtained quantitative USAXS results confirm clearly the anisotropic character of the porosity at EB-PVD TBCs, especially at the Q ranges between 0.00149 and 0.01285 (corresponding to a main opening dimension of 420nm and 48nm, respectively) (see Table II). These features display somewhat smaller growth-orientation angles (42°) at the microstructures "intermediate" and "feathery". The size distribution of the different pores was in some cases so broad, that these have to be modeled in two separated void populations. These result show that the thickness of the inter-columnar gaps at all investigated microstructures lie in the range of 602-670nm in as-coated conditions, making 4.08% - 8.38% of volume fraction. In the case of feather-arm openings, there are two representative dimensional ranges for the microstructures "intermediate" and "coarse, whereas only one dimension for the microstructure "feathery". Their volume fraction is a factor of four or higher at the microstructures "intermediate" and "coarse" (5.39% and 9.56%, respectively) than that at the microstructure "feathery" (1.40%). The measured coarser opening dimensions for the feather-arm features are given in the following after the schema [diameter/thickness (aspect ratio)]. It is found that these are 1.3/0.12μm (0.09) at the microstructure "intermediate", 1.6/0.15μm (0.09) at the microstructures "coarse" and 1.8/0.09μm (0.05) at the microstructure "feathery". Furthermore, the finer dimensional range for the "intermediate" and "coarse" is represented with 0.7/0.05μm (0.07) (see Table II).

Finally, the intra-columnar pores in the three investigated coatings show also two dimensional ranges. Although these can not be packed into specific dimensional groups being representative for all three coatings, nevertheless, it is distinctive that there is one group of intra-columnar pores yielding prolate ellipsoid shape (aspect ratio = 20) at all coatings. The dimension of those at the microstructure "coarse" (0.4/0.02μm) is approx. twice as large as those in the other two microstructures, counting solely for the smallest volume fraction (5.80%). It is noticeable that a higher volume fraction (19.82%) of the porosity at the microstructure "feathery" corresponds to these prolate ellipsoid shaped intra-columnar pores [diameter/thickness = 0.17/0.008μm]. Moreover, the intra-columnar pores at the microstructure "intermediate" fall in their dimension and volume fraction (0.2/0.01μm and 11.63%) between those of the other two microstructures. These pores are mostly located as aligned rows behind the voids between feather-arms and, thus, oriented at the same angles as the feather-arm voids (see Table II and Fig. 3). The second group of intra-columnar pores display a disc shape with an intermediate aspect ratio value. These are also oriented at similar angles as the feather-arms. The determination of the pore shapes has been carried out by fitting the modelling curves with those of the measured USAXS scattering curves, since each of the modelling shapes (oblate ellipsoid, sphere, and prolate ellipsoid) affects the shape factor P(Q) of the measured scattering intensities I(Q) by modifying the slope of fitted curves[20].

The USAXS results for the coatings in the as-coated state can be summarised as such that the "feathery" microstructure contains the finest dimension and highest volume of intra-columnar pores followed by the "intermediate" and finally by the "coarse" microstructure. Thus, due to their dimensions and aspect ratios, it can be assumed that, on thermal exposure, the intra-columnar pores of the first opening dimension are predestined to break into quasi-spherical pores due to the occurrence of sintering process[21].

By considering the pores as thermal insulators (i.e. insignificant radiation contribution), it can be stated that the spatial and geometrical distribution of all pore types at EB-PVD TBCs will

contribute, according to their effectiveness, to the reduction of the thermal conductivity by interruption of phonon flow through the coating. This means that, as well as the finer dimensions, the higher volume of these cylindrical intra-columnar pores contributes significantly in thermal conductivity reduction of EB-PVD TBCs. This hypothesis is supported by the fact that this relationship defined by USAXS-modeling analysis agrees well with those experimentally determined thermal conductivity values of the three as-coated microstructures (see Fig. 4).

In the case of the microstructures "intermediate" and "coarse", larger intra-columnar pore sizes are anticipated and measured due to the applied lower rotation speeds during processing. Moreover, since these microstructures are manufactured at higher substrate temperatures, only a fraction of these pores are able to form at each rotation phase and will only survive until the next array of new pores are created. These both coatings consist of a lower volume fraction of intra-columnar pores which are heterogeneously distributed. Thus, it is plausible that their measured thermal conductivity values are higher.

After heat treatment at 1100°C for 100 hours, the sintering process becomes active, leading to morphological changes at all pore types[3]. Mass transfer occurs through bridging at the contact points between primary columns forming two dimensional groups of inter-columnar pores. This phenomenon is enhanced by the fact that the finer columns, which are cumulated mostly at the bottom zone of the coating and interrupted from growing through the coating thickness, tend to pull together and create finer channels between them. The volume fraction of such fine inter-columnar gaps is higher at the microstructures "feathery" and "intermediate" (15.58% and 14.08%, respectively) than those at the microstructure "coarse" (8.55%) (see Fig. 5).

On ageing, significant changes occur at the finer feather-arm regions and intra-columnar pores. The effect of sintering is obvious, considering the decrease in the USAXS-modeled aspect ratios which is controlled by the surface area reduction of the pores. The dimension group addressing the finer gaps disappears completely after ageing. These break into arrays of quasi-spherical pores at their inner pyramidal ends, leaving isolated openings with lower aspect ratio at the edge of the feather-arms. The secondary columns of feather-arm features appear to sinter into groups, leaving broader but shorter gaps between the feather-arms (see Fig. 5).

Finally, high aspect ratio cylindrical intra-columnar pores (e.g. fine "banana" shaped pores) which are created at each rotation phase and connect the two pore rows break into quasi-spherical pores (see Fig. 6). Moreover, on ageing, the volume fraction of these pores is drastically reduced, especially at the microstructure "feathery" from 19.82% in the as-coated state to 5.41% after heat-treatment. Consequently, a different equilibrium configuration of the pores results from the sintering process altering the effectiveness of the pores in interruption of the heat transfer through the coatings.

Considering the changes at the thermal conductivity of the coatings after heat-treatment at 1100°C/100h (Fig. 4) and in their morphological changes (Figs. 3 and 6), it can be clearly stated that the changes at the intra-columnar cylindrical pores, aligned behind the feather-arm features are responsible for the drastic thermal conductivity increase in the microstructure "feathery". These changes occur not only in their shape (from prolate ellipsoids to quasi-spheres) but also in their volume fraction, resulting in a decrease reaching to nearly a factor four (from 19.82% to 5.41%). Their significant influence can be attributed to the disappearance of heat-flux hindering paths and formation of isotropic features which facilitate heat transfer.

CONCLUSIONS

In this study employed USAXS-analysis supported with modeling was able to quantitatively and rather accurately determine the geometry and location of anisotropic voids within the three EB-PVD TBC microstructures in the as-coated and aged conditions. The variation of the EB-PVD process parameters produces evident differences in the spatial and geometrical characteristics of the porosity within the manufactured TBCs. Also the heat treatment of these at 1100°C/100h induce irreversible thermal activated processes (i.e. sintering), modifying the distribution and geometry of the pores. According to the results of the thermal conductivity measurements and those from the USAXS–modeling, it is discernible that the intra-columnar pores are the principal constructors of the heat-flux (phonons) through the coatings enhanced by their high volume concentration and distribution.
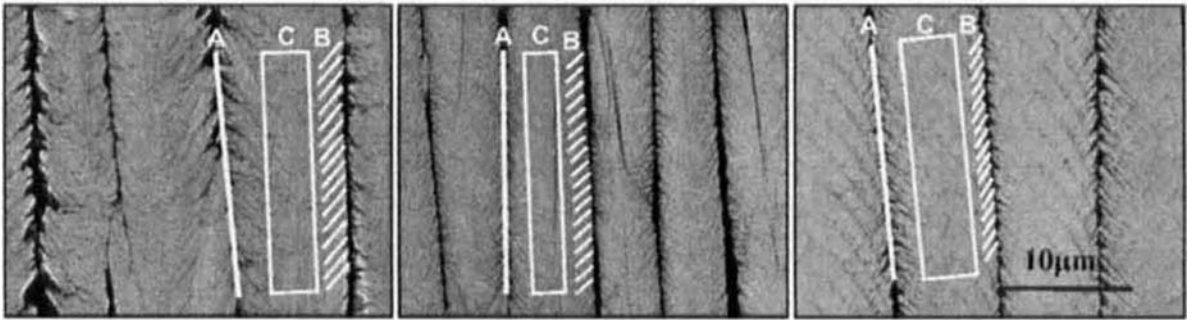


**Figure 1:** Scanning electron micrographs of EB-PVD TBCs cross sections at the direction perpendicular to the PVI showing the inter-columnar pores (A), pores between feather-arms (B) and intra-columnar pores (C): feathery (left), intermediate (middle), and coarse (right).
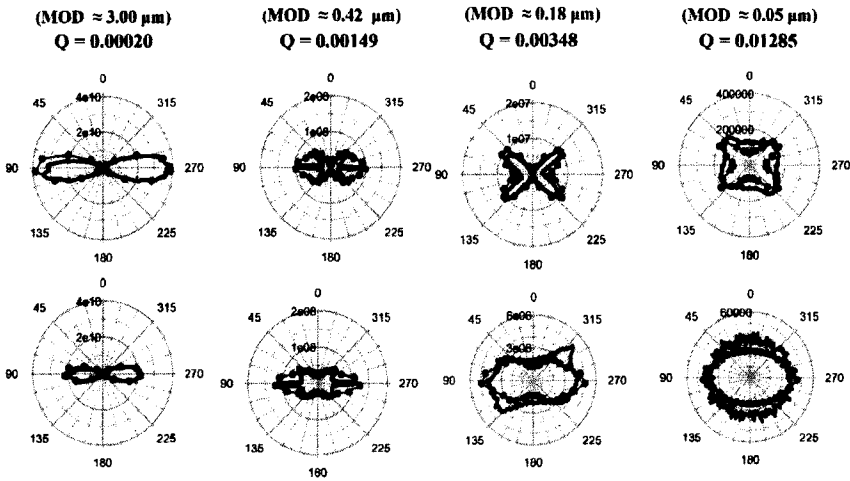
**Figure 2:** Measured (——) and modeled ( —●—) polar distribution of the USAXS-scattered intensities versus the azimuthal angle (α) at different Q values and the corresponding main open dimensions (MOD) for the "coarse" microstructure in cross-section perpendicular to PVI: (a) as-coated and (b) after heat treated conditions at 1100°C/100h.

Table II: Calculated values of spatial and geometrical characteristics of the porosity within the three analyzed EB-PVD TBCs in as coated and after ageing conditions via USAXS-modelling.

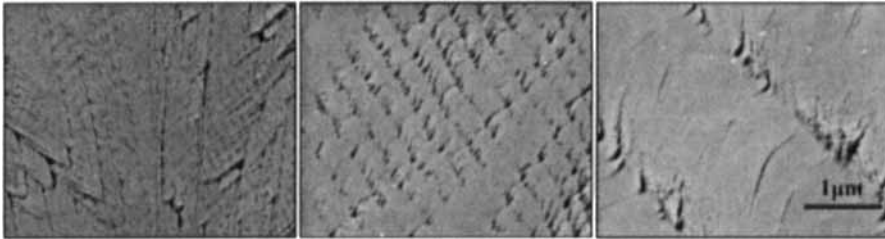| Pore type as-coated "Intermediate" | Ellipsoidal Shape | Azimuthal angle | Diameter (nm) | Thickness (nm) | Aspect Ratio | Volume fraction |
|---|---|---|---|---|---|---|
| Inter-columnar-1 | Oblate | 82 | - | 673.00 | 0.05 | 8.38 |
| Between feather-arms-1 | Oblate | 42 | - | 118.30 | 0.091 | 1.21 |
| Between feather-arms-2 | Oblate | 42 | 705.70 | 45.87 | 0.065 | 4.18 |
| Intra-columnar-1 | Prolate | 42 | 13.00 | 260.00 | 20.00 | 11.63 |
| Intra-columnar-2 | Oblate | 42 | 33.50 | 15.10 | 0.45 | 1.74 |
| Pore type heat-treated "Intermediate" | Shape | Azimuthal angle | Diameter (nm) | Thickness (nm) | Aspect Ratio | Volume fraction |
| Inter-columnar-1 | Oblate | 84 | - | 469.18 | 0.05 | 8.65 |
| Inter-columnar-2 | Oblate | 84 | - | 124.80 | 0.26 | 5.43 |
| Between feather-arms-1 | Oblate | 45 | 580.00 | 174.00 | 0.30 | 3.08 |
| Intra-columnar-1 | Oblate | 45 | 120.52 | 84.36 | 0.70 | 4.65 |
| Intra-columnar-2 | Oblate | 45 | 44.00 | 35.20 | 0.80 | 5.32 |
| Pore type as-coated "coarse" | Shape | Azimuthal angle | Diameter (nm) | Thickness (nm) | Aspect Ratio | Volume fraction |
| Inter-columnar-1 | Oblate | 86 | - | 602 | 0.05 | 5.92 |
| Between feather-arms-1 | Oblate | 54 | - | 154.11 | 0.095 | 2.78 |
| Between feather-arms-2 | Oblate | 54 | 718.65 | 53.907 | 0.075 | 6.78 |
| Intra-columnar-1 | Oblate | 54 | 210.17 | 63.05 | 0.30 | 1.26 |
| Intra-columnar-2 | Prolate | 54 | 22.31 | 446.33 | 20.00 | 5.80 |
| Pore type heat-treated "coarse" | Shape | Azimuthal angle | Diameter (nm) | Thickness (nm) | Aspect Ratio | Volume fraction |
| Inter-columnar-1 | Oblate | 92 | - | 563.00 | 0.05 | 7.05 |
| Inter-columnar-2 | Oblate | 92 | - | 156.00 | 0.26 | 1.50 |
| Between feather-arms-1 | Oblate | 54 | 872.75 | 174.55 | 0.20 | 4.95 |
| Intra-columnar-1 | Oblate | 54 | 261.30 | 209.04 | 0.80 | 5.27 |
| Intra-columnar-2 | Oblate | 54 | 51.43 | 46.28 | 0.90 | 3.78 |
| Pore type as-coated "feathery" | Shape | Azimuthal angle | Diameter (nm) | Thickness (nm) | Aspect Ratio | Volume fraction |
| Inter-columnar-1 | Oblate | 84 | - | 602.45 | 0.07 | 4.08 |
| Inter-columnar-2 | Oblate | 84 | - | 61.70 | 0.14 | 2.14 |
| Between feather-arms-1 | Oblate | 42 | 1868.80 | 93.44 | 0.05 | 0.60 |
| Between feather-arms-2 | Oblate | 42 | 222.71 | 31.18 | 0.14 | 0.80 |
| Intra-columnar-1 | Prolate | 42 | 8.58 | 171.71 | 20.00 | 19.82 |
| Pore type heat-treated "feathery" | Shape | Azimuthal angle | Diameter (nm) | Thickness (nm) | Aspect Ratio | Volume fraction |
| Inter-columnar-1 | Oblate | 88 | - | 591.33 | 0.05 | 4.48 |
| Inter-columnar-2 | Oblate | 88 | - | 85.00 | 0.22 | 11.10 |
| Between feather-arms-1 | Oblate | 52 | 1467.36 | 161.41 | 0.11 | 1.14 |
| Intra-columnar-1 | Oblate | 52 | 123.45 | 98.76 | 0.80 | 5.31 |
| Intra-columnar-2 | Oblate | 52 | 37,36 | 29,88 | 0,80 | 5.41 |

**Figure 3:** Scanning electron micrographs of EB-PVD TBCs cross sections at the direction perpendicular to the PVI showing the intra-columnar pores: feathery (left), intermediate (middle), and coarse (right).
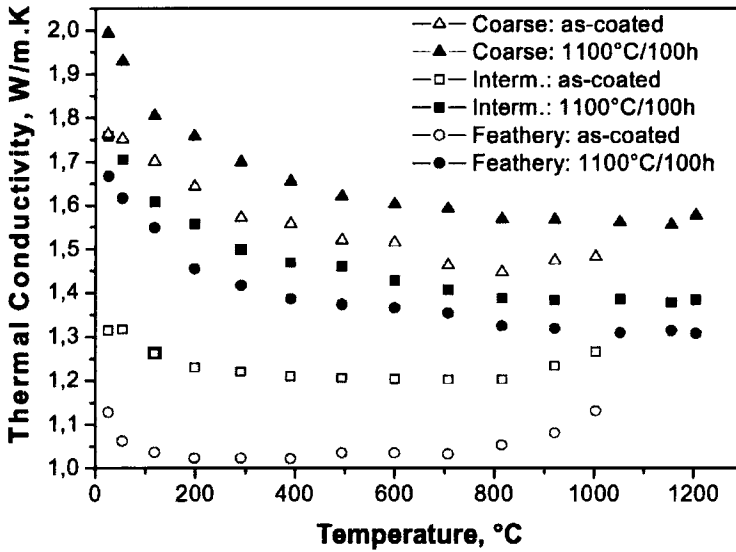


**Figure 4:** Thermal conductivities vs. measuring temperature values of the three analyzed microstructures: feathery, intermediate and coarse.
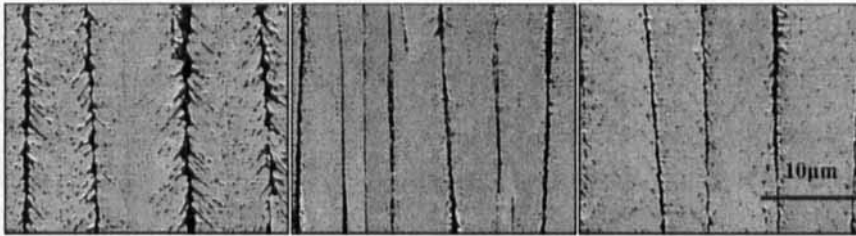
**Figure 5:** Scanning electron micrographs of heat treated (1100°C/100h) EB-PVD TBCs cross sections after heat treatment at the direction perpendicular to the PVI: feathery (left), intermediate (middle), and coarse (right).
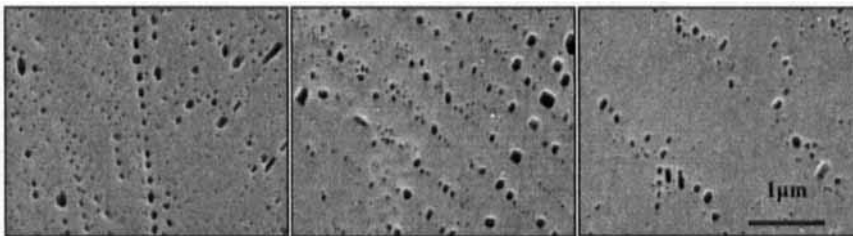


**Figure 6:** Scanning electron micrographs of heat treated (1100°C/100h) EB-PVD TBCs cross sections at the direction perpendicular to the PVI showing the intra-columnar pores: feathery (left), intermediate (middle), and coarse (right).

REFERENCES

[1] S.G. Terry, Evolution of microstructure during the growth of thermal barrier coatings by Electron-Beam Physical Vapor Deposition, Materials Department, University of California, Santa Barbara, 2001, p. 197.
[2] A.F. Renteria, B. Saruhan, U. Schulz, H.-J. Raetzer-Scheibe, Effect of Morphology on Thermal Conductivity of EB-PVD PYSZ TBCs, Surface and Coatings Technology, accepted for publication, (2006).
[3] A.F. Renteria, B. Saruhan, Effect of ageing on microstructure changes in EB-PVD manufactured standard PYSZ top coat of thermal barrier coatings, Journal of the European Ceramic Society, in Press, Vol.: 26, (2006).
[4] H.-J. Ratzer-Scheibe, U. Schulz, T. Krell, The effect of coating thickness on the thermal conductivity of EB-PVD PYSZ thermal barrier coatings, Surface and Coatings Technology In Press, Corrected Proof (2005).

[5]U. Schulz, C. Leyens, K. Fritscher, M. Peters, B. Saruhan-Brings, O. Lavigne, J.-M. Dorvaux, M. Poulain, R. Mévrel, M. Caliez, Some recent trends in research and technology of advanced thermal barrier coatings, Aerospace Science and Technology, 7, 73-80 (2003).

[6]C.G. Levi, Emerging materials and processes for thermal barrier coatings, Current Opinion in Solid State and Materials Science, 8, 77-91 (2004).

[7]T.A. Dobbins, A.J. Allen, J. Ilavsky, G.G. Long, A. Kulkarni, H. Herman, P.R. Jemian, Recent developments in the characterization of anisotropic void population in thermal barrier coatings using ultra-small angle x-rays scattering, in: Ceram. Eng. and Sci. Proc. (ed. by W.M. Kriven, H.-T. Lin), The American Ceramic Society, pp. 517-524 (2003).

[8]J. Ilavsky, A.J. Allen, G.G. Long, P.R. Gemian, Effective pinhole-collimated ultrasmall-angle x-ray scattering instrument for measuring anisotropic microstructures, Review of scientific instruments, 73, 1-3 (2002).

[9]A.J. Allen, Characterization of ceramics by x-ray and neutron small-angle scattering, J. Am. Ceram. Soc., 88, 1367-1381 (2005).

[10]J. Ilavsky, A.J. Allen, A. Kulkarni, T. Dobbins and H. Herman, Microstructure characterization of thermal barrier coatings deposits - practical models from measurements, in: E. Lugscheider, A. International, M. Park (Eds.), International Thermal Spray Conference, Basel, Switzerland, 2005.

[11]U. Schulz, S.G. Terry, C.G. Levi, Microstructure and texture of EB-PVD TBCs grown under different rotation modes, Materials Science and Engineering A 360, 319-329 (2003).

[12]U. Bonse, M. Hart, An X-ray interferometer with long separated interfering beam paths, Appl. Phys. Lett., 7, 99-100 (1965).

[13]A.J. Allen, J. Ilavsky, G.G. Long, J.S. Wallace, C.C. Berndt, H. Herman, Microstructural characterization of yttria-stabilized zirconia plasma-sprayed deposits using multiple small-angle neutron scattering, Acta Materialia, 49, 1661-1675 (2001).

[14]G. Porod, General theory, in: O. Glatter, O. Kratky (Eds.), Small-angle X-rays scattering, Academic Press, London, (1982).

[15]J.S. Pedersen, Form factors of block copolymer micelles with spherical, ellipsoidal and cylindrical cores, J. Appl. Cryst., 33, 637-640 (2000)

[16]G. Beaucage, Approximations leading to a unified exponential/power law approach to small-angle scattering, J. Appl. Cryst., 28, 717-728 (1995).

[17]A.J. Allen, S. Krueger, G. Skandan, G.G. Long, H. Hahn, H.M. Kerch, J.C. Parker, M.N. Ali, Microstructure evolution during sintering of nanostructured ceramic oxides, J. Am. Ceram. Soc.,9, 1201-1212 (1996).

[18]D. Marchal, B. Demé, Small- angle neutron scattering by porous alumina membranes of aligned cylindrical channels, International Union of Crystallography, pp. 713-717 (2003)

[19]D. Sen, A.K. Patra, S. Mazumder, S. Ramanathan, Pore morphology in sintered $ZrO_2$-$_8$% mol $Y_2O_3$ ceramic: a Small-Angle Neutron Scattering investigation, Journal of Alloys and Compounds, 340, 236-241 (2002).

[20]R.-J. Roe, Small-Angle Scattering, in: J.E. Mark (Ed.), Methods of X-ray and neutron scattering in polymer science, Oxford University Press, New York, pp. 155-209 (2000).

[21]J.S. Stoelken, A.M. Glaeser, The morphological evolution of cylindrical rods with anisotropic surface free energy via surface diffusion, Scripta Metallurgica et Materialia, 27, 449-454 (1992).